Charmo Journal of Natural Sciences and Technologies (CJNST)

CJNST 2025, Vol. 2, Issue 1, pp. 30–43

https://cjnst.chu.edu.iq/

Research Article:

Vegetation Health Classification in the Kurdistan Region Using AI and Sentinel-2A Satellite Data

Shnow Abdl Qader Muhamad[1]*, Safar Maghdid Asaad[2], Zrar Khalid Abdul[1]

[1]Computer Department, College of Science, Charmo University, Sulaymaniyah, Iraq.
[2] Department of Software Engineering, Faculty of Engineering, Koya University, Danielle Mitterrand Boulevard, Koya 44023, Kurdistan Region, Iraq

https://doi.org/10.31530/cjnst.2026.2.1.3

Received: 31 January 2026
Revised: 27 February 2026
Accepted: 7 March 2026

***Corresponding author info:** Shnow Abdl Qader Muhamad (shno.abdulqar@chu.edu.iq)

Abstract

Background: Monitoring climate science is imperative, as it provides the scientific information needed on current changes in the Earth's climate system and their environmental and ecological consequences. However, precisely and scalably classifying vegetation health in heterogeneous semi-arid regions is challenging, particularly with limited labeled data and computational resources.

Aims: This study develops an effective vegetation health classification model using Sentinel-2 imagery and machine learning. This paper examines vegetation health assessment as an ecological indicator of environmental stress, rather than climate change prediction perse.

Methodology: A Support Vector Machine (SVM) classifier was trained using vector histogram features extracted from the Sentinel-2A spectral bands (B2, B3, and B4), and its hyperparameters were tuned via Bayesian optimization to achieve optimal performance. The model was trained and evaluated on 379 images from the Kurdistan Region, belonging to three vegetation health classes (moderately healthy, unhealthy, and dead).

Results: The proposed method achieved 90.79% test accuracy, outperforming Convolutional Neural Network (CNN), Random Forest (RF), and K-Nearest Neighbors (KNN) baselines while maintaining low computational complexity.

Conclusion: These findings highlight the effectiveness of compact spectral representations for accurate and efficient vegetation health classification, supporting scalable monitoring in resource-constrained semi-arid regions.

Keywords: Deep Learning, Environmental Monitoring, Feature Engineering, Machine Learning, NDVI, Remote Sensing, Sentinel-2A, SVM, Vegetation Health Classification.

1. Introduction

Vegetation health monitoring has become increasingly important in the context of climate change, which affects precipitation and temperature regimes, with consequent impact on plant productivity and global distribution [1]. Frequent droughts, land degradation, and intensive anthropogenic activities have rapidly accelerated the regression of vegetation in many semi-arid regions. The Kurdistan Region of Iraq (KRI) is a typical example of a semi-arid Mediterranean climate. Such changes compromise agriculture, biodiversity, and ecosystem services, underscoring the urgent need for rapid, spatially explicit assessments of plant health to support land-use planning and climate adaptation strategies. Accurate mapping of vegetation is important for sustainable natural resource management and the mitigation of climate change [2] since vegetation affects CO_2 uptake, the hydrological cycle, and soil conservation [1], [3].

Vegetation monitoring has been revolutionized by remote sensing technology, enabling large-scale, regular surveys of the Earth's surface. Sentinel-2 has improved performance in terms of spatial resolution (10 m), temporal resolution (5-day revisit), and number of spectral bands (13) compared to other systems such as Landsat [4], [5]. These properties make Sentinel-2 ideally suited for fine-resolution vegetation studies, such as health monitoring and land-cover classification [6]. The vegetation types and spectral overlap among classes vary in semi-arid regions, making

classification difficult and necessitating advanced methods that can account for nonlinear and multiscale relationships in the data.

With the rapid expansion of computing resources, machine-learning (ML) approaches are more efficient and can process large, high-dimensional remote sensing data for improved vegetation monitoring [7]. ML approaches such as RF, SVM, and KNN have shown strong efficacy in vegetation classification using spectral indices and reflectance data [8], [9]. Model prediction accuracy depends largely on the amount and representativeness of the training samples [10]. Recently, Deep Learning (DL) techniques such as CNN have shown strong capability for capturing complex spatial patterns in remote sensing imagery [11]. CNNs may outperform conventional ML models on large, homogeneous datasets; however, they are computationally expensive and require substantial labelled data. In cases of limited data or complex environments, traditional classifiers, such as RF and SVM, can outperform CNNs [11].

This analysis is based on the idea that vegetation health assessment can serve as a possible ecological indicator of environmental stress, rather than predicting climate change. The study focuses on computing Normalized Difference Vegetation Index (NDVI)-based vegetation parameters and on generating a vector-histogram model to improve classification accuracy. Several models from SVM, RF, KNN, and CNN are built and compared using a unified protocol to identify the most effective approach. The study tests the empirical performance of these models using test datasets and ultimately proposes a scalable, cost-effective tool to support regional vegetation monitoring and data-driven environmental management.

The present study makes a significant contribution to the field of remote sensing for vegetation analysis. First, the methodology employs a hybrid AI-based strategy that integrates vector-histogram features derived from NDVI in Sentinel-2A data with ML (SVM, RF, and KNN) and DL (CNN) models to classify vegetation health. This method demonstrates better classification accuracy and computational efficiency on a moderate-sized heterogeneous regional database. Second, it offers the first holistic application of AI-based vegetation health modelling for KRI, filling a key geographical gap in the literature. Finally, the study provides a scalable, repeatable method that can be adapted to other resource-limited ecosystems for informed environmental planning, drought risk reduction, and land management policy development.

The rest of this paper is organized as follows. The Related work is described in Section 2. Data collection, preprocessing, feature extraction, and the construction of ML and DL models are described in the proposed methodology (Section 3). Section 4 introduces and discusses the experimental results, assesses model performance across a range of classifiers, and compares the results with the current state of the art. Section 5, Conclusion, summarizes the main results and possible extensions.

2. Related Work

Monitoring vegetation health is in great demand for environmental monitoring, agricultural production management, and land-use evaluation. The most frequently applied techniques to achieve this objective are NDVI classification using threshold values and visual interpretation of satellite images. However, such technologies typically have issues with accuracy and scalability, particularly in heterogeneous environments. Advances in AI and remote sensing have enabled automated, more accurate classification methods. Table 1 presents all related works on vegetation health classification.

Landsat satellites have been the most important source of satellite image data for the past decades because of their long-term temporal archive. Their spatial resolution of 30 meters and return cycle of 16 days make them suitable for capturing long-term trends. However, they are limited in detecting subtle changes in vegetation health, especially in dense and heterogeneous landscapes. Similarly, the Moderate Resolution Imaging Spectroradiometer (MODIS) has a relatively low spatial resolution (250–1000 meters) and a high repeat frequency (1–2 days), thereby limiting its application for fine-scale detection of changes in vegetation condition. For example, in [3], Generalized Linear Models (GLMs) were used to analyze vegetation resilience using Landsat data, without traditional categorical labels, whereas [2] classified vegetation using MODIS NDVI time series and climatic data. However, these studies primarily considered continuous NDVI dynamical and resilience metrics rather than conducting multi-class vegetation health classification, due to the lack of an explicit definition of vegetation health, which continues to create a gap in practical health-focused classification at the regional scale.

To address these limitations, ML methods, including SVM and RF, have been consistently employed to improve the accuracy of Landsat-based land-use and land-cover classification. For instance, RF and SVM were combined to classify land use in geothermal regions using Landsat and Sentinel-2 multispectral imagery, along with spectral indices including NDVI, Normalized Difference Built-up Index (NDBI), and Normalized Difference Water Index (NDWI), to achieve high classification accuracy and enable sustainable water management [12]. Similarly, in [13], Multinomial Logistic Regression (MLR) was applied to Landsat data to generate land-use and land-cover maps at the national scale in India. While ML approaches improved LULC mapping accuracy, they also classified land cover types in general terms rather than vegetation health categories.

The spatial resolution (10 meters) and temporal revisit (5 days) of Sentinel-2 significantly improve MODIS and Landsat. The enhanced capacity enables greater monitoring of dynamic ecosystems, including urban, forest, and agricultural environments. In [5], RF was used for land-cover classification in the Arctic, employing 41 features, including NDVI, red-edge bands, and topographic metrics. In [14], the authors used multi-temporal Sentinel-2 imagery with an SVM to classify eight types of mountain vegetation in Poland, achieving an overall accuracy of 80%. In [6], Sentinel-2 and SVM were used to evaluate the health of

grassland areas in South Africa. An overall accuracy of 90.5% (excellent results) was reported when RF was used to map vegetation in Portugal [8]. In [9], RF regression was applied to Sentinel-2 data to predict the chlorophyll fluorescence in olive trees (R^2 = 0.752, RMSE = 0.078). These studies showed that Sentinel-2 is suitable for vegetation classification in both temperate and polar regions. However, these did not mention health condition assessment, and their adaptability to semi-arid regions with spectral features remains unvalidated.

It has been proven that multisource methodologies are beneficial. In this regard, RF, SVM, and classification and regression tree (CART) techniques were used to classify birch, larch, and non-forest regions using integrated unmanned aerial vehicle (UAV), Sentinel-2, and light detection and ranging (LiDAR) data, with RF outperforming all other models, achieving 79% accuracy for Scheme I and 86% for Scheme II (with canopy height model (CHM)). Features used included spectral bands, vegetation indices (NDVI, Enhanced Vegetation Index (EVI)), texture (Grayscale Symbiosis Matrix), and vertical structure (CHM) [15]. Despite the performance gains of multisource fusion, LiDAR data were expensive and unsuitable for large-area monitoring. Moreover, spectral features derived from histograms have not yet been studied for vegetation health classification.

The vegetation monitoring has shown significant advancements in DL algorithms. The authors implemented Long Short-Term Memory (LSTM) networks and an Entity-Aware LSTM (EA-LSTM) on these MODIS-derived data, achieving a drought classification accuracy of 78.3% in Kenya [16]. Using multi-date Sentinel-2 data, they employed a pixel-based recurrent CNN and achieved an overall classification accuracy of over 96.5% for multi-class land and crop classification [4]. Among these, the work of [17] evaluated the ability of Conv1D, GoogLeNet, and Contextual Guidance Network (CGNet) to classify 10 vegetation types in a subtropical region based on Sentinel-2 time stamps. CGNet achieved the highest F1-score (0.90), indicating that fusing spectral and temporal information works well.

The study [18] addressed forest cover classification in the Abbottabad, Pakistan, case study area using a model designed for Sentinel-2 images. This research achieved high classification accuracy (97.75% for ANN and 96.98% for RF). Although DL methods can effectively learn temporal patterns for classifying vegetation types, they require substantial computational resources and labeled data. Their applicability for estimating health states in data-deficient contexts is unclear.

Despite substantial progress in applying ML and DL to vegetation monitoring, several gaps remain. First, limited work has evaluated vegetation health classification using Sentinel-2 imagery in semi-arid environments such as the Kurdistan Region, where spectral responses differ from temperate ecosystems. Second, most prior studies have focused on land cover classification or vegetation type mapping rather than multi-class vegetation health gradients. Third, while spectral indices and texture features have been widely explored, histogram-based spectral representations remain largely unexamined for multi-class health classification.

To address these gaps, this study proposes an SVM-based framework using histogram features derived from Sentinel-2 bands (B2, B3, B4) for vegetation health classification in the Kurdistan Region.

Table 1: Summary of related studies on vegetation health classification

Study	Data Source(s)	Objectives / Focus	Labels (Classes)	Methods	Features	Results
[2]	MODIS-Terra	Vegetation and land use classes	Irrigated farming Dry farming Rich rangelands Moderate rangelands.	Statistical trend analysis	NDVI, temperature, precipitation, land use/land cover maps	Precipitation mainly influences plant growth rate, while temperature has minimal impact.
[3]	Landsat	Analyzing vegetation resistance to increasing aridity in global drylands	No discrete labels	GLM	NDVI, species richness, soil moisture, soil texture, bare soil fraction, elevation, drought history	About 21.6% of global drylands crossed aridity thresholds between 2000 and 2022
[5]	Sentinel-2	Land-cover classification for Arctic regions in Greenland	9 land-cover types	RF	41 features including vegetation indices (e.g., NDVI, NDMI), red-edge bands, phenological metrics, and topographical features	overall accuracy:91.8%

[8]	Sentinel-2	Vegetation mapping in Lousã, Portugal	10 vegetation classes: Pinus pinaster, Eucalyptus, Quercus, Castanea, Acacia, Pinus pinea, Cropland, Shrubland, Water, Barren	RF	NDVI, GNDVI, EVI, SAVI	Overall accuracy: 90.5%
[12]	Landsat 8 and Sentinel-2	Land use monitoring	urban areas and vegetation, water bodies and forests	SVM, RF	NDVI (vegetation), NDBI (built-up index), NDWI (water index), plus spectral bands	SVM: 2023 = 0.93 RF: 2023 = 0.97
[13]	Landsat	LULC mapping, India.	LULC categories: forest, agriculture, water, built-up, barren land	Multinomial Logistic Regression	NDVI, Spectral bands	Accuracy: 80% to 86% across all years
[14]	Sentinel-2	Mountain vegetation classification in Giant Mountains, Poland.	Bogs and fens, Deciduous shrub vegetation, Forests, Grasslands, Heathlands, Subalpine tall forbs, Subalpine dwarf pine scrubs, Rock and scree vegetation	SVM	Spectral bands, vegetation indices, PCA	overall accuracy 80% using multi-temporal datasets
[6]	Sentinel-2A/B multispectral	Grassland biome fragmentation analysis (2016, 2019, 2023)	Grassland, Forest, Water, Agriculture, Other (urban/mining)	SVM	Multispectral bands from Sentinel-2 (13 bands with 10m to 60m resolution), Vegetation Indices (NDVI, MSAVI2, OSAVI, NDRE), and spectral signatures	accuracy 97.62% in 2016, 97.66% in 2019, 98.58% in 2023.
[9]	Sentinel-2	Chlorophyll fluorescence prediction (Fv′/Fm′) in olive trees	Not applicable (continuous target)	RF, SVR, GBM, EN, KNN, DT, LM	Sentinel-2 Bands	RF highest accuracy with R^2 = 0.752, RMSE = 0.078
[15]	UAV, Sentinel-2, LiDAR	Tree species classification	Birch, Larch, Non-forest	SVM, CART, RF	NDVI, EVI, GLCM, CHM from LiDAR	RF is the best Scheme I: 79%, Scheme II: 86%
[16]	MODIS	drought monitoring in Kenya	Drought severity	EA-LSTM	NDVI-derived VCI, precipitation, evaporation, soil moisture, altitude, month of year	Accuracy: 78.3%

[4]	Sentinel-2	Land cover and crop classification	13 crop types: Tomatoes Artificial Surfaces, Trees, Rye, Wheat, Soybean, Apple, Pear, Grassland, Water, Lucerne, Durum Wheat, Vineyard, Barley, Maize	Pixel R-CNN	Multispectral bands (Blue, Green, Red, NIR), NDVI, Temporal sequences	Accuracy: 96.5%
[17]	Sentinel-2	Vegetation classification	10 classes: Eucalyptus plantation, Mangrove, Other broadleaf forest, Mixed broadleaf-conifer forest, Loquat, Jujube, Honey pomelo, Farmland, Grassland, Non-vegetation	Conv1D, GoogLeNet, CGNet	Sentinel-2 multispectral time series data, 1D time series, 2D recurrence plot images, spectral bands (e.g., red edge, NIR), temporal features	Overall accuracy F1. score Conv1D: 0.85, GoogLeNet: 0.87, CGNet: 0.90
[18]	Sentinel-2	Forest cover classification and monitoring	Fields, Forest, Shrubs, Urban	ANN, RF	Single-layer and temporal layer stacked multispectral Sentinel-2	ANN Acc: 97.75%, RF Acc: 96.98%

3. Methodology

This study employs a series of combination stages (satellite imagery, cloud-based processing, feature extraction, and ML to categorize vegetation health in KRI. As illustrated in Figure 7, this process involves multiple steps, including data acquisition, preprocessing of the acquired data, feature extraction, and adapting CNN and ML algorithms to classify whether vegetation is healthy.

3.1. Data Collection

Given its ecological and topographic diversity, including rolling mountains, settlement areas, and agricultural lands (KRI), the research area was chosen to represent vegetation types. Figure 1 displays the study region in KRI, and the blue circles indicate the sample Sentinel-2A image patches (not all) used for this study.

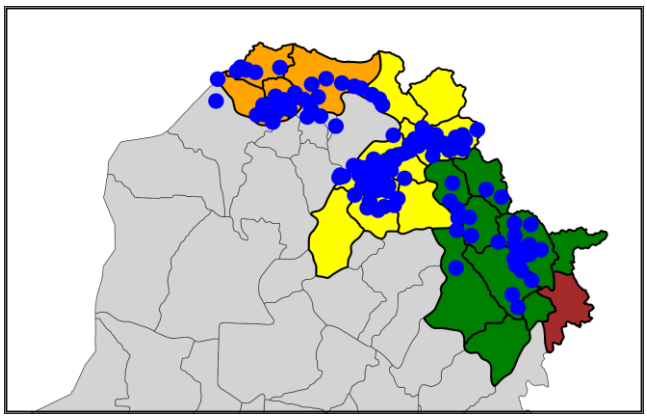

Figure 1. Study area at KRI

Then, due to this heterogeneity, remote sensing-based vegetation classification techniques can be compared consistently. The region's environmental variability facilitates the assessment of vegetation health across a range of biophysical conditions.

The Sentinel-2A satellite, provided by the European Space Agency (ESA), is already considered the primary source of satellite imagery for this research. The Sentinel-

2A's Multispectral Instrument (MSI) acquires imagery in 13 spectral bands at spatial resolutions of 10m, 20m, and 60 m. In this study, we extract images from the Sentinel-2A satellite using Google Earth Engine (GEE). GEE offers up-to-date, trustworthy satellite data, combined with modern tools, to enhance spectral data processing and analysis.

Accordingly, 379 images covering a total area of 2 km² were captured from different locations within KRI. To maintain spatial regularity and computational efficiency, each Sentinel-2A scene was resampled to a 2 km² resolution. This spatial scale was used as a compromise between sufficient representation of vegetation heterogeneity and workable file sizes for processing.

No particular season was focused on; images were collected across multiple seasons to improve the generalization and robustness of the proposed system. Sample locations in KRI were selected randomly to achieve a representative coverage. Once the imagery in GEE had been cropped using JavaScript-based tools, image patches were stored as 8-bit RGB thumbnails (67 x 54 pixels) in GeoTIFF format using the visualize () function. Although the default spatial resolution of Sentinel-2 bands is 10 m, this value reflects the GEE export settings rather than the sensor's spatial resolution. The 379-image dataset used a compressed format to reduce memory usage while still allowing the retrieval of visual patterns of vegetation for ML classification. The dataset was split into training and testing sets using an 80:20 ratio to ensure robust model evaluation. The dataset comprises 379 Sentinel-2 image patches collected across the Kurdistan Region. An image-level split was applied to ensure separation between training and testing data. Because all patches originate from the same geographical region, some spatial autocorrelation may remain despite random sampling, which is a known limitation in regional remote sensing studies. Figure 2 represents the Red Band (B4) images of the three vegetation health classes in the Kurdistan Region dataset.

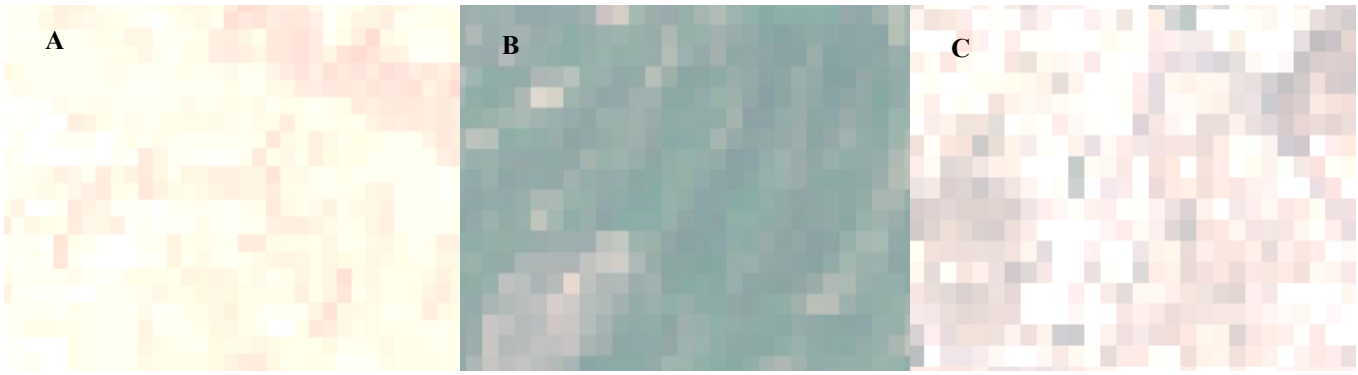

Figure 2: Original Red Band (B4) samples representing the three classes: (A) Dead plant, (B) Moderately healthy plant, (C) Unhealthy plant

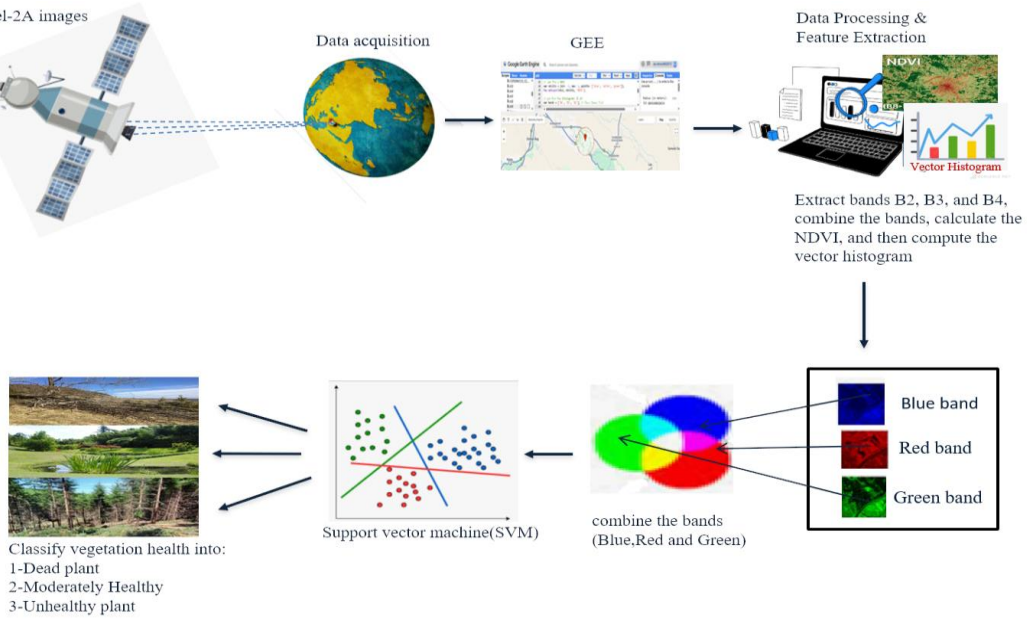

Figure 3: Proposed framework for vegetation health classification in the KRI

Figure 4 shows the proposed research flowchart for vegetation health classification. It illustrates the steps from Sentinel-2A image acquisition, preprocessing, NDVI calculation, and feature extraction to the final vegetation health assessment. The obtained images were then labeled in three vegetation health categories of Dead, Unhealthy, and moderately Healthy plants according to NDVI thresholds calculated at the preprocessing phase.

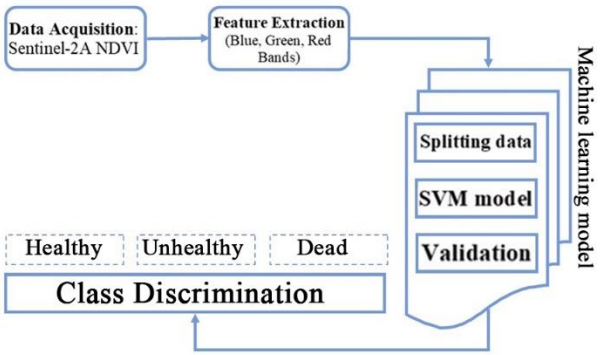

Figure 4: Flowchart of the proposed vegetation health classification

3.2. Data Preprocessing

Preprocessing is necessary to maintain accuracy and align the images with the expectations of vegetation classification. Following the retrieval of image data, all satellite imagery is first georeferenced and then temporally and spatially standardized to maintain consistency throughout the dataset. This ensures they are aligned for pixel-level analysis and comparison. Two important spectral bands used in NDVI calculation, which are B4 (red, 665 nm) and B8 (near-infrared, 842 nm) [9], with 10m spatial resolution, were used for vegetation health assessment. Those bands are commonly used to determine the NDVI and are important for vegetation analysis.

The NDVI is a consistent indicator of vegetation health in the research area and is computed from selected spectral bands using Equation (1).

The NDVI formula applied to these images gives very precise information about the plant health, whether it is dead, unhealthy, or moderately healthy, and the NDVI provides very good information about the environmental factors affecting the vegetation of Kurdistan.

$$NDVI = \frac{B8\,(NIR) - B4\,(Red)}{B8\,(NIR) + B4\,(Red)} \qquad (1)$$

Red is the red band of the image, and the near-infrared (NIR) band. NDVI values range from -1 to +1, providing a quantitative index of vegetation condition: high values typically indicate healthier vegetation, while low values indicate less dense or stressed vegetation. The NDVI-based thresholds to classify vegetative states used in the following description are:

NDVI < 0.05 is categorized as a Dead Plant.

0.05 < NDVI < 0.2 is indicated as an Unhealthy Plant.

0.2 < NDVI < 0.6 is classified as a Moderately healthy Plant.

These thresholds are consistent with NDVI classes reported in multiple studies [2], [3], [8] were further validated empirically through NDVI distribution analysis in GEE during data preprocessing.

After sorting the images, additional preprocessing steps were performed. The analysis uses Sentinel-2 Level-2A surface reflectance products, which are atmospherically corrected using the Sen2Cor processor. Scenes with more than 20% cloud coverage were excluded using the CLOUDY_PIXEL_PERCENTAGE metadata filter. Reflectance values were rescaled by dividing by 10,000 to convert digital values to surface reflectance. Finally, median compositing was applied to reduce residual cloud contamination, shadow effects, and radiometric noise. The NDVI indices and corresponding spectral bands are stored as structured datasets. Image data are converted to vectorized histograms to compactly represent the spatial and spectral patterns, which are useful for subsequent analysis. This process efficiently maintained the feature extraction and vegetative structure. The pixel intensity distribution of Red Band (B4) for all vegetation health classes is presented in Figure 5 after the preprocessing.

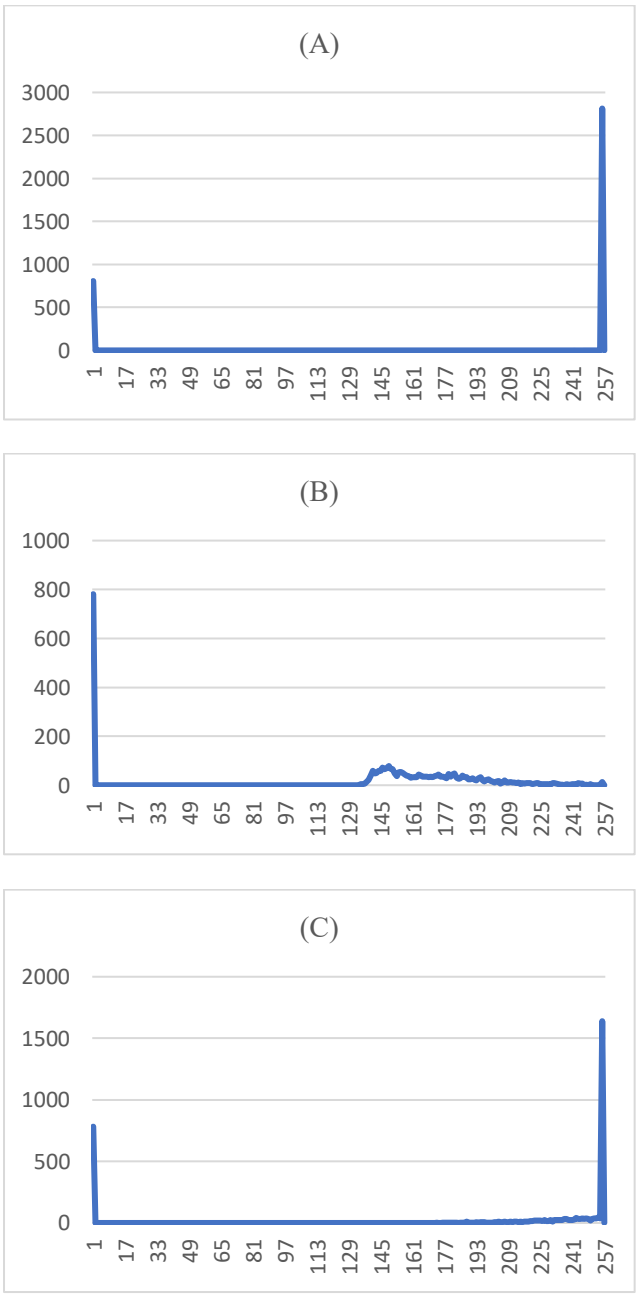

Figure 5: Red Band (B4) vector histograms showing pixel intensity values across the three classes, where (A) Dead plant, (B) Moderately healthy plant, and (C) Unhealthy plant

3.3. Feature Extraction

The next important step in preprocessing is to develop meaningful features that can accurately classify vegetation health conditions. Histogram-based features were selected to provide a compact and interpretable spectral representation that reduces dimensionality while preserving vegetation-related spectral distributions, making them suitable for moderate-sized remote sensing datasets. The feature extraction entails using the Sentinel-2A Bands B2 (Blue), B3 (Green), and B4 (Red) to build a full set of features for training the model.

A vector histogram method is applied to quantify the spectral features. The pixel intensity distribution for each band is used to obtain a unique vector histogram. In addition to these single-band histograms, scatter plots for pairwise bands are generated to represent the joint spectral response between B2 & B3, B2 & B4, and B3 & B4. Finally, the three-band combination (B2, B3, and B4) is also computed for the complex relationship among the visible channels.

These histograms, built over picture patches or pixel areas, represent the texture, color, and state of vegetation by encoding the frequency distributions of spectral intensities. Linear and non-linear relationships between bands, often related to plant health, can be represented using combination histograms. The resulting feature space includes:

Histograms with only one band: B2, B3, and B4

Combinations in pairs: B2-B3, B2-B4, and B3-B4

Combination of all bands: B2-B3-B4

3.4. Classification Model: SVM

The extracted features are fed into SVM, a supervised ML model suitable for high-dimensional classification tasks. The goal of SVM is to identify the hyperplane that best separates features into different classes.

Vector histograms of the individual bands, all pairwise band combinations, and finally, combined as a whole to make up the input features for the SVM model. These histograms serve as compact, discriminative representations of spectral characteristics and are aggregated across image regions.

Experimental Setup and Hyperparameter-Tuning

To perform proper training and testing of the model on new data. The dataset consists of two parts: training and testing. Model parameters were learned on 80% of the training set. The test set, which contains 20% of the data, is used to evaluate how well the trained model generalizes. This standard practice still holds the unseen samples for performance evaluation, while enabling the model to learn on a representative subset of the data

Additionally, the research uses a Bayesian optimization strategy to fine-tune hyperparameters rather than a random search. Bayesian optimization stores exploration of the hyperparameter space in a lightweight surrogate model, such as a Gaussian process. The details of the Bayesian optimization are presented in Table 2.

Table 2: Hyperparameter tuning using Bayesian optimization configuration

Parameter	Description
Framework	BayesSearchCV from scikit-optimize with Bayesian optimization based on Gaussian Process
Search Space - C	Real: [1e-6, 1e+6] (log-uniform prior)
Search Space - Kernel	Categorical: {linear, rbf, poly, sigmoid}
Search Space - Gamma	Categorical: {scale, auto}
Search Space - Degree	Integer: {2, 3, 4, 5}
Number of Iterations	20 hyperparameter configurations
Cross-Validation	3-fold stratified K-fold
Evaluation Metric	Classification accuracy (maximized)
Parallel Processing	Multi-core (n_jobs=-1)

The SVM-based parameters listed below are adjusted based on the Bayesian optimization method to optimize classification performance with the associated dataset splitting:

C: The regularization parameter, which strikes a balance between classification error and margin width. Degree: Polynomial kernel degree; comes into play only when the kernel is set to 'poly'. Gamma: Indicates how much each training sample (either "auto" or "scale") has an impact. (only applicable to rbf, poly, and sigmoid kernels).

Kernel: The kind of decision function (linear, poly, or rbf), rbf stands for Radial Basis Function, a kernel mapping input to a higher-dimensional space to help with target nonlinearities [19].

Table 3 summarizes the optimized hyperparameter values for each band and their combinations. The term "Combine " is used to provide all three spectral bands (Blue Band from Band2, Green Band from Band3, and Red Band from Band4) as a single feature, combining spectral bands into a composite feature set for a classification process. Note: NIR band (B8) is not part of this combination. To assess the impact of different feature sets on the model performance, we also tested pairwise combinations (B2-B3, B2-B4, B3-B4) and single-band histograms (B2, B3, B4).

Table 3: SVM hyperparameter settings for each band and combinations

Bands	C	Degree	Gamma	Kernel
Blue	2.2376	N/A	scale	rbf
Red	0.8745	N/A	auto	rbf
Green	3.1406	N/A	auto	rbf
Blue-Green	4.6253	N/A	auto	rbf
Blue-Red	0.1098	N/A	N/A	linear
Red-Green	0.0114	N/A	N/A	linear
Combine	20.8706	N/A	scale	rbf

4. Results and Discussions

This section explains and discusses the findings of the SVM classification model for vegetation health in KRI. Classification is performed on single spectral bands (Blue, B2; Green, B3; Red, B4), two bands' combination taken at a time (B2-B4, B2-B3, and B4-B3), as well as through the combination of all three bands. The purpose of the analysis is to identify which choices can effectively distinguish the healthy status of the vegetation.

Strong empirical evidence is provided by the results in Table 4, which show how different spectral bands and their combinations affect the SVM classifier for vegetative health classification. We report both test and training accuracies to provide insight into how well the model generalizes. This dual reporting is necessary to learn certain problems, such as (1) underfitting, where accuracies on the training and test sets are low, (2) overfitting, where training accuracy is high but test accuracy is low, and (3) data scarcity, which often leads to unstable learning. There appears to be a small amount of overfitting, as the blue band decreased in test accuracy (78.95% with high loss 21.05%), while training accuracy remained relatively high at 88.12%. It appears that the blue band can capture some vegetation characteristics at the training point, but it is not discriminative enough to make reliable generalizations.

In contrast, the red band displayed equally balanced losses (17.16% vs. 17.11%) and almost identical accuracy between training and testing, with average values of 82.84% and 82.89%, indicating a good generalized model. This stability could be due to the strong correlation between the red band and chlorophyll absorption, making it a good choice for vegetation extraction. The green band achieved high generalization, with training and test accuracies of 84.82% and 80.26%, respectively. However, its higher test loss (19.74%) may indicate overfitting or reduced separability when working only in this band.

Significant improvement was observed when specific band combinations were used. A slight drop in training accuracy from 87.29% led to better test accuracy, with a clear reduction in test loss to 15.79%. This enhancement indicates that combining these two bands can provide additional spectral information,

enabling the classifier to distinguish vegetation health statuses. More importantly, the Blue-Red combination performed better than any of the bands alone, achieving a test accuracy of 86.18% and a test loss of 13.82% (including low values). This result illustrates how effectively the pigment-sensitive blue band and the chlorophyll-sensitive Red band complement one another to improve spectral contrast. Despite having a lower training accuracy of 80.03.

The best performance was obtained with the combination of three bands (Blue, Green, and Red). The most important thing is that the model trained on all features reached a peak test accuracy of 90.79% and a minimum test loss of 9.21%, with even better training precision of 99.01%. The rich, multi-scale profile information stored in vector histogram features may underlie the model's remarkable generalization and stability. The relatively small gap between test and training performance shows that the model did not just overfit the data but also generalized meaningful patterns. Overall, the study's outcomes confirm that the SVM can capture the complexity of spectral variations associated with vegetation health status in KRI, particularly when supplemented with feature combinations and Gaussian-approximated hyperparameter tuning.

Table 4: SVM classification performance using vector histogram features from individual bands, band pairs, and combined bands.

Bands	Training Accuracy	Training Loss	Test Accuracy	Test Loss
Blue	88.12%	11.88%	78.95%	21.05%
Red	82.84%	17.16%	82.89%	17.11%
Green	84.82%	15.18%	80.26%	19.74%
Blue-Green	87.29	12.71	84.21	15.79
Blue-Red	85.81	14.19	86.18	13.82
Red-Green	80.03	19.97	84.21	16.45
Combine	99.01%	0.99%	90.79%	9.21%

This matrix presents a clear, structured view of the model's ability to discriminate vegetation health classes, showing which are misclassified correctly.

In this setup:

Class 0 corresponds to Moderately Healthy Plants,

Class 1 to Unhealthy Plants, and

Class 2 to Dead Plants.

As illustrated in the figure, the model performed very well at identifying Moderately Healthy Plants (Class 0); all 35 of its samples were classified without error, indicating that it is confident in its classification. In the Dead Plant class (Class 2), the model also achieved good results, with a total of 20 correct classifications and only 2 mislabeled as Unhealthy. It indicates how well, though not decisively, the mode and its dataset discriminate stressed vegetation.

However, the Unhealthy Plant class (Class 1) had the highest misclassification rate. Of 14 samples, 14 were accurately classified, three were incorrectly labeled as Dead Plants, and two were predicted as Moderately Healthy Plants. This confusion could be attributed to the partial overlap of the spectral responses of moderately healthy vegetation with those of the other two land cover types when the vegetation is under intermediate stress, which are spectrally subtle.

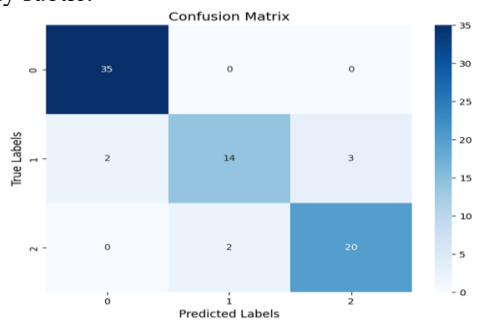

Figure 6: Confusion matrix of the SVM model using combined spectral bands.

As shown in Table 4, the SVM model produced the best classification accuracy when the combined spectral bands (B2, B3, and B4) were used. To provide a fair and uniform evaluation framework, this ideal combination was therefore kept for all ensuing model comparisons. In this regard, the end-to-end workflow for vegetation health classification using (A) CNN on raw Sentinel-2 images and (B) classical ML models SVM, RF, KNN, and CNN on vector histogram features is depicted in Figure 7, which also provides a comparative diagram of the implemented approaches. The variations in preprocessing and learning techniques across the studies help readers visually understand the methodological differences and the rationale for each model's performance.

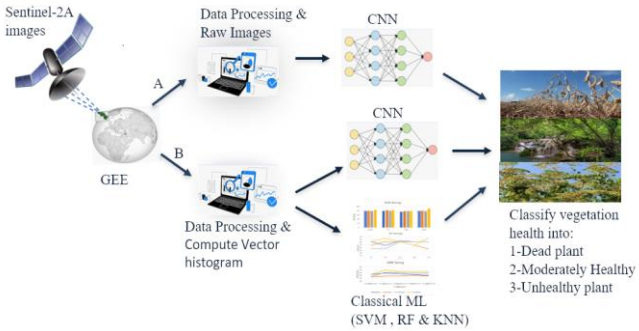

Figure 7: CNN and classical ML model-based approaches for vegetation health classification

A. Comparison with Traditional ML Models

Under the same feature configuration, the suggested SVM model outperformed two popular traditional classifiers, RF and KNN, with a test accuracy of 90.79% utilizing the combined bands, as illustrated in Table 5. In particular, the RF model and KNN both performed worse than SVM, with accuracies of 85.53% and 88.16%, respectively.

To ensure a fair comparison, both RF and KNN models were fine-tuned using a systematically applied Bayesian optimization approach. The RF classifier proved to be the best model with max_depth = 10 and n_estimators = 173, but was surpassed by KNN using a Manhattan distance metric with k = 3. Despite these varied parameters, the large range consistently suggests that SVM captured realistic, complex relations better in the spectral data (especially when using histogram-based features), but was not worse than KNN. Even though RF is built on an ensemble framework, it did not perform well, presumably because of its sensitivity to high-dimensional feature correlations.

Table 5. Accuracy of traditional ML models using combined spectral bands (B2, B3, B4)

Models	Accuracy %
SVM	90.79
KNN	88.16
RF	85.53

B. Comparison with CNN

A CNN using the same set of attributes, in histogram form, was tested to compare with the SVM method. KNN performance was comparable to the 1D CNN model, which scored lower than SVM, with a test accuracy of 88.16. This result suggests that histogram features may not conform to the spatial learning assumptions of CNNs in a limited-data setting. Bayesian optimization was employed to optimize the CNN model to improve its performance. The filter progression (128, 32, 256) was learned with automatic hyperparameter search by Bayesian optimization (Optuna). The optimized architecture and training setup for 1D and 2D CNN models are shown in Table 6.

As shown in Table 7, the 2D CNN model's lower accuracy (81.27%) may be attributed to several factors, including the relatively small training dataset, differences in feature representation, and the applied training configuration. In particular, CNNs are typically most effective when large datasets are available and when spatial patterns can be learned directly from raw imagery. In contrast, the histogram-based features used in this study provide structured spectral information that may be more suitable for moderate-sized datasets. As DL methods are often chosen for their capacity to learn complex hierarchical representations directly from pixels without human control, this experiment using raw image data could help examine the end-to-end learning ability of CNNs. Bayesian optimization was also used for this model version. Even with this adjustment, the CNN's accuracy was reduced, suggesting that structured feature representations, such as histograms, are more effective on moderate-sized remote sensing datasets.

Table 6: Optimized CNN architecture and training configuration

Configuration Detail	1D CNN (Vector Histogram)	2D CNN (Raw Images)
Backbone Architecture	Custom CNN (not pre-trained)	Custom CNN (not pre-trained)
Number of Conv Layers	3	3
Conv Layer 1 (filters, kernel)	128 filters, kernel=3	16 filters, kernel=(3,3)
Conv Layer 2 (filters, kernel)	32 filters, kernel=3	96 filters, kernel=(3,3)
Conv Layer 3 (filters, kernel)	256 filters, kernel=3	256 filters, kernel=(3,3)
Number of Dense Layers	1 (256 units)	2 (256, 32 units)
Activation Functions	ReLU (Conv, Dense), Softmax (output)	ReLU (Conv, Dense), Softmax (output)
Pooling Strategy	MaxPooling1D (pool_size=2) after Conv2 & Conv3	MaxPooling2D (pool_size=2×2) after each Conv
Optimizer	Adam	Adam
Learning Rate	Bayesian-optimized [1e-4, 1e-2]	Bayesian-optimized [1e-4, 1e-2]
Loss Function	Categorical Crossentropy	Categorical Crossentropy
Input Normalization	StandardScaler	Rescale (÷255)

Regularization	None	None
Batch Size	32	32
Number of Epochs	10	Up to 20 (early stopping)
Data Augmentation	None	None
Early Stopping	No	Yes (monitor=val_loss, patience=3, restore_best_weights=True)

To evaluate whether the proposed framework can be applied to compute impedances for different land cover classes, we included 72 additional Sentinel-2A images corresponding to different land types as an external test set, bringing the total to 451. The best-performing model was the support vector machine, with 95.83% accuracy, indicating strong generalization potential. In contrast, the 1D CNN model achieved slightly lower accuracy (93.06%), likely due to the small size of the training dataset. A few urban and road areas with dead vegetation were removed to reduce the class imbalance in the dataset. Although the SVM performed better than the CNN in our experiment, this is expected because of the dataset size (medium-sized), which generally favors SVMs that effectively handle structured numerical features such as vector histograms. The CNN model could benefit from a larger dataset, ideally with over 500 images per class and a broader study area. However, CNN models demand greater computational resources. An exception to this is the poorer performance, which also illustrates that statistically designed features, such as vector histograms, exhibit greater generalization and discriminative power than raw-spectrum input in this particular classification test.

Table 7: Accuracy of DL models using vector histograms (combined spectral bands (B2, B3, B4)) and raw satellite images

Models	Feature Type	Accuracy %
SVM	Vector Histogram (VH)	90.79
CNN (VH)		88.16
CNN (Raw Satellite)	Raw Pixels	81.27

To assess whether the observed performance differences are statistically significant on the same test set, we applied McNemar's test using paired predictions. The SVM showed a statistically significant improvement over CNN (Raw Satellite) (McNemar's exact test, p =0.04), indicating that the accuracy difference is unlikely to be due to chance on the evaluated test samples.

Figure 8 shows the CNN's learning pattern after training on raw satellite images. As can be observed, there are indications of overfitting: the training accuracy continues to improve, while the validation accuracy fluctuates considerably after the sixth epoch. Likewise, after initially declining, the validation loss increases, which is consistent with the previously noted reduced test accuracy of 81.27%. This result demonstrates that, unlike the SVM model, which used structured vector histogram features, the CNN struggled to generalize from raw pixel inputs.

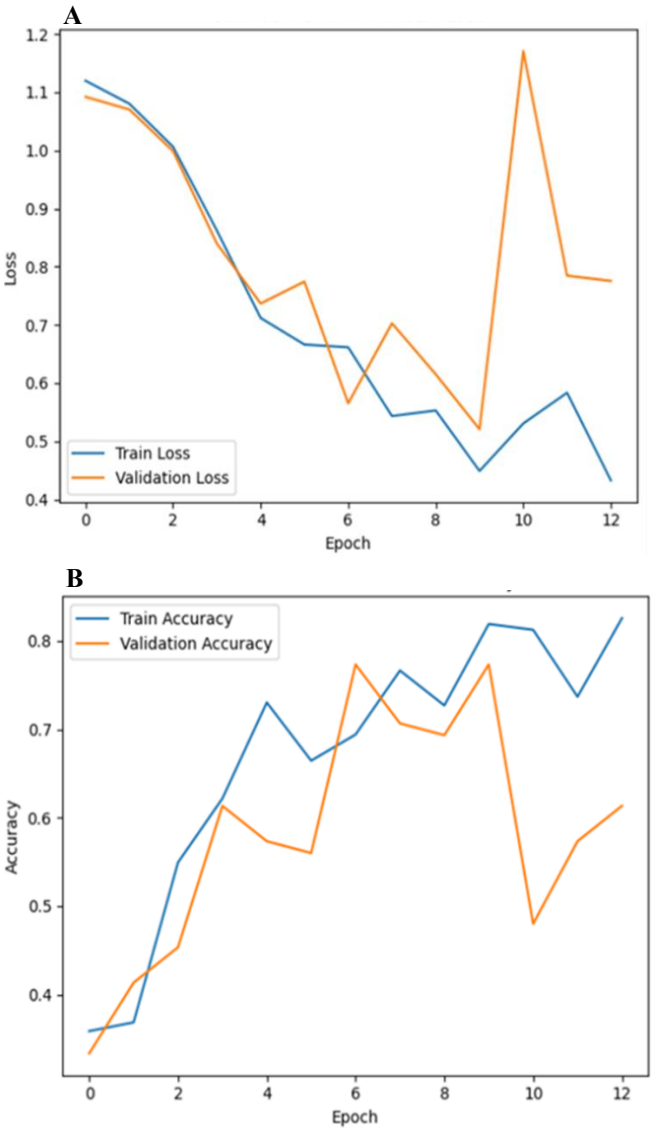

Figure 8: Training and validation accuracy/loss curves for the CNN model using raw satellite images: (A) CNN using raw image – Loss, (B) CNN using raw image - Accuracy

Figure 9 summarizes the accuracy results of several models using the combined spectral bands and shows how well the proposed SVM model performs compared to both CNN and traditional ML methods (RF, KNN). As shown, the SVM model achieves the best accuracy of 90.79%, followed by KNN and CNN. In contrast, Raw-image CNNs had lower accuracy, likely due to limited access to training data.

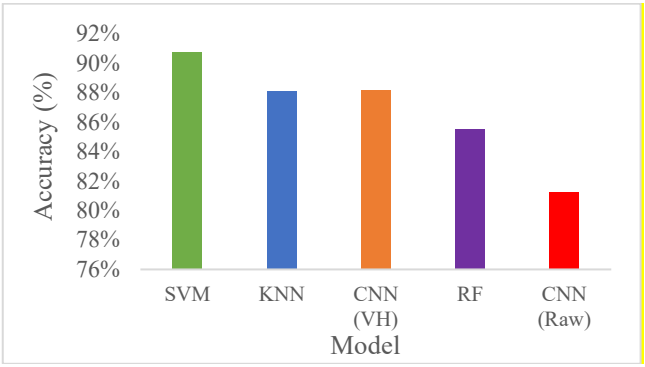

Figure 9: Accuracy comparison of SVM, KNN, RF, and CNN models using combined spectral bands.

In this study, multiple diagnostic indicators, including sensitivity, specificity, precision, recall, and F1-score, were investigated to evaluate the performance of the SVM-based classification model. These statistics are important for addressing an imbalance in the distribution of vegetation health classes. Sensitivity and specificity estimates for three classes of plant health: Moderately Healthy (Class 0), Unhealthy (Class 1), and dead (Class 2) are provided in Table 8. The outstanding ability of the SVM model in accurately recognizing healthy plant samples is also indicated by its 100% sensitivity for Class 0. Furthermore, it showed good sensitivity for Class 1 (73.68%), which is also the hardest category to recognize across all models, and excellent sensitivity for Class 2 (90.91%). There was no class for which the SVM's specificity fell below 94%, indicating that it can reduce false positives. The SVM achieved the best performance across both sensitivity and specificity, particularly in difficult mid-green vegetation cases.

Table 8: Sensitivity and Specificity performance of classification algorithms for vegetation health

Algorithm	Metric	Class 0	Class 1	Class 2
SVM	Sensitivity	100.0%	73.68%	90.91%
	Specificity	95.12%	96.49%	94.44%
RF	Sensitivity	94.29%	57.89%	95.45%
	Specificity	90.24%	94.74%	92.59%
KNN	Sensitivity	100.0%	52.63%	100.0%
	Specificity	87.80%	100.0%	92.59%
CNN	Sensitivity	94.29%	68.42%	95.45%
	Specificity	95.12%	94.74%	92.59%

Additionally, a complete analysis of Precision, Recall, and F1 Scores is also presented in Table 9. In Class 0, the SVM model led the test with an F1-score of 97.22%, indicating its accuracy and reliability in recognizing relatively healthy vegetation. SVM had an 80.00% F1-score with a stunning precision (87.50%) and was also superior to others in the case of more pleaded Class 1 (Unhealthy). In addition, SVM maintained good performance on Class 2 (Dead vegetation) with an F1-score of 88.89%. Other models, including CNN and KNN, performed well but with lower reliability, especially for Class 1 precision and sensitivity. The difference shows that the SVM model is reliable across different vegetation conditions and achieves the best overall accuracy (90.79%).

Table 9: Evaluation metrics of classification algorithms across classes.

Algorithm	Metric	Class 0	Class 1	Class 2
SVM	F1-Score	97.22%	80.00%	88.89%
	Precision	94.59%	87.50%	86.96%
	Recall	100.00%	73.68%	90.91%
RF	F1-Score	91.67%	66.67%	89.36%
	Precision	89.19%	78.57%	84.00%
	Recall	94.29%	57.89%	95.45%
KNN	F1-Score	93.33%	68.97%	91.67%
	Precision	87.50%	100.00%	84.62%
	Recall	100.00%	52.63%	100.00%
CNN	F1-Score	94.29%	74.29%	89.36%
	Precision	94.29%	81.25%	84.00%
	Recall	94.29%	68.42%	95.45%

C. Comparison with State-of-the-Art Approaches

A comparison was made with the state-of-the-art methodology, which employed different satellite sensors, classification algorithms, and feature extraction techniques to validate the effectiveness of the proposed vegetation health classification model. A summary of results across datasets, study areas, vegetation types, and classifiers is presented in Table 10.

The classification results indicate that the proposed approach, combining Sentinel-2 imagery with an SVM classifier and histogram encoding of the B2, B3, and B4 bands, achieved 90.79% accuracy across three levels of vegetation health (Dead, Unhealthy, and Moderately Healthy). This performance is competitive with several traditional ML and DL approaches reported for related vegetation classification tasks.

The study in [13] used MLR with Landsat data and achieved accuracies between 80–86% for different land-use/land-cover (LULC) classifications. While covering a broader range of terrain types, the results reflect differences in both the target task and sensor characteristics. Similarly, [14] reported an average accuracy of 80% for mountain vegetation types using Sentinel-2 and SVM with multi-temporal inputs and vegetation indices.

By using RF and Sentinel-2 imagery in Portugal, [8] achieved a precision of 90.5% across 10 vegetation types. Their results are relatively similar to ours, but comparisons may be difficult because they used a more extensive set of

vegetation indices (NDVI, Green Normalized Difference Vegetation Index (GNDVI), EVI, and Soil-Adjusted Vegetation Index (SAVI)). Nevertheless, the proposed model uses three basic bands linked via histogram encoding, making it easier to interpret and more computationally efficient.

In [17], a benchmark of DL was conducted using different CNNs, including Conv1D, GoogLeNet, and CGNet, on Sentinel-2 time series. The proposed model's accuracy is similar to that of CGNet, their best-performing model, which obtained an F1-score of 0.90. However, these approaches often required larger amounts of training data and greater computational resources and relied on more complex temporal and spectral characteristics, including red-edge and NIR bands.

In [18], forest cover classification/LULC mapping (4 classes: Forest/Fields/Shrubs/Urban) in Abbottabad, Pakistan, achieved 97.75% (ANN) and 96.98% (RF) using temporal Sentinel-2 stacking (4 dates). However, this represents LULC land cover classification rather than a 3-class vegetation health assessment (Healthy/Unhealthy/Dead), making direct accuracy comparison inappropriate due to differences in task objectives and label space.

In contrast, the proposed SVM model is an interpretable, low-complexity solution that is particularly useful for regional-scale vegetation monitoring (e.g., in the KRI), where IT infrastructure may be limited.

CNN-based models, including those trained directly on raw Sentinel-2 images, were also analyzed within the proposed framework. CNNs did not match the performance of SVMs with engineered features, but still achieved respectable results (81.27% accuracy with raw image input). In remote sensing, this difference underscores that manually engineered features, such as vector histograms, still outperform feature-learning methods.

McNemar's test is only applicable to models evaluated on the same test instances with available paired predictions; therefore, statistical significance testing is reported for the internal baselines trained and tested on our dataset, whereas Table 10 provides a contextual cross-study comparison where paired testing is not possible.

Table 10: Comparison of SVM-based vegetation classification with state-of-the-art approaches

Study	Satellite	Target Classes	Algorithm	Features Used	Performance	Model complexity	Train time	Inference time	Memory	Data size
[8]	Sentinel-2	Vegetation type (Portugal)	RF	NDVI, GNDVI, SAVI, EVI	90.5%	NR	NR	NR	NR	NR
[13]	Landsat	LULC (India)	Multinomial Logistic Regression	NDVI, spectral bands	80–86%	NR	NR	NR	NR	NR
[14]	Sentinel-2	Mountain vegetation types	SVM	Spectral bands, indices, PCA	80%	NR	NR	NR	NR	NR
[17]	Sentinel-2	Classify 10 vegetation types (China)	Conv1D, GoogLeNet, CGNet	Time-series bands, NIR, Red Edge	85%–90% (F1-score)	NR	NR	NR	NR	NR
[18]	Sentinel-2	Forest cover classification/ LULC map	ANN, RF	temporal layer stacked	ANN Acc: 97.75%, RF Acc: 96.98%	NR	NR	NR	NR	NR
Proposed	Sentinel-2	Vegetation Health (Kurdistan)	SVM	Vector Histogram of B2, B3, B4	90.79%	768 features, 162 support vectors (per class)	0.0238 s	0.151372 ms/sample (0.011504 s/run on test set)	2.74 MB (training peak), 10.35 MB (optimization peak)	379 images (80/20split)

NR: Not reported in the original study. Report the feature dimension and the number of support vectors as measures of practical complexity for SVM. The SVM-based vegetation health classification approach developed in this study can be useful for local authorities to detect drought conditions and plan irrigation and to prioritize intervention areas in semi-arid systems. In combination with land-use data, the model's outputs can subsequently be used to guide optimal crop distribution, understand ecosystem stress, and support an adaptive management approach. Through these applications, the developed system provides a practical utility and suitability for agricultural planners, environmental land managers, and other local practitioners.

This study has some limitations despite its encouraging results. The moderate dataset size, the restriction to a single region (KRI), and the absence of species-level vegetation categorization may limit the generalizability of DL models. The study did not target specific plant species but rather the general vegetation type. Future multi-index fusion (SAVI, EVI, red-edge indices) will enhance classification robustness in semi-arid conditions. Future research will address these constraints by expanding the framework in several

ways, including expanding its coverage to all Iraqi territories. First, the temporal continuity and geographical granularity of vegetation health evaluations are expected to be enhanced by integrating multi-temporal and multi-sensor data sources (e.g., Sentinel-1, hyperspectral, and LiDAR images). As evidence, similar frameworks have been successfully used in other fields, for example, in tree species classification, where promising results were achieved [15]. Second, to reduce reliance on large amounts of labeled data and enhance the model's generalizability across diverse ecological zones, transfer learning and semi-supervised learning will be explored. Third, adding supplementary information, such as topography, soil type, and climate conditions, might improve classification. Lastly, the establishment of a cloud-based, real-time monitoring platform aims to facilitate proactive environmental decision-making at the regional and national levels and to enable ongoing vegetation observation.

5. Conclusions

This study focuses on vegetation health assessment as a potential ecological indicator of environmental stress, rather than direct climate change prediction. The proposed SVM-based framework has achieved superior performance compared to other traditional ML methods, RF, KNN, and DL techniques, CNN, for the comparative experimental settings with an accuracy of 90.79% by utilizing NDVI-based labelling in combination with vector histogram feature engineering, and by employing SVM classifier tuned through Bayesian optimization tricks. Compact, discriminative spectral features enhanced classification accuracy and reduced computational load, rendering the method applicable in a resource-limited environment. The model also performed well in identifying severely damaged vegetation, with an excellent receiver operating characteristic and high sensitivity and specificity across all levels of vegetation health.

In addition to its technical contribution, this study fills a significant geographic and scientific gap by focusing on the ecologically sensitive, topographically complex area of the KRI. This area is underrepresented in the remote sensing literature. Results offer actionable insights for climate adaptation strategies, land use planning, and environmental policy in KRI.

6. References

[1] S. Usman, J. O. Jayeoba, and A. Kundiri, "Climate change as a global concept: Impacts and adaptation measures," *International Journal of Environment and Climate Change*, vol. 14, no. 6, pp. 445–459, 2024. doi:10.9734/ijecc/2024/v14i64242.

[2] A. Bagherzadeh, A. V. Hoseini, and L. H. Totmaj, "The effects of climate change on normalized difference vegetation index (NDVI) in the northeast of Iran," *Modeling Earth Systems and Environment*, vol. 6, no. 2, pp. 671–683, 2020. doi:10.1007/s40808-020-00724-x.

[3] C. Abel *et al.*, "Vegetation resistance to increasing aridity when crossing thresholds depends on local environmental conditions in global drylands," *Communications Earth & Environment*, vol. 5, no. 1, 2024. doi:10.1038/s43247-024-01546-w.

[4] V. Mazzia, A. Khaliq, and M. Chiaberge, "Improvement in land cover and crop classification based on temporal features learning from Sentinel-2 data using recurrent convolutional neural networks," *Applied Sciences*, vol. 10, no. 1, 2020. doi:10.3390/app10010238.

[5] D. A. Rudd, M. Karami, and R. Fensholt, "Towards high-resolution land-cover classification of Greenland: A case study covering Kobbefjord, Disko and Zackenberg," *Remote Sensing*, vol. 13, no. 18, 2021. doi:10.3390/rs13183559.

[6] A. Netsianda, P. Mhangara, and E. Gidey, "Grassland biome fragmentation analysis using Sentinel-2 images and a support vector machine learning model in South Africa," *Discover Sustainability*, vol. 5, no. 1, 2024. doi:10.1007/s43621-024-00723-3.

[7] A. A. Abdullah, N. S. Mohammed, M. Khanzadi, S. M. Asaad, Z. K. Abdul, and H. S. Maghdid, "In-depth analysis of machine learning approaches: Techniques, applications, and trends," *ARO – The Scientific Journal of Koya University*, vol. 13, no. 1, pp. 190–202, 2025. doi:10.14500/aro.12038.

[8] P. Mohammadpour, D. X. Viegas, and C. Viegas, "Vegetation mapping with random forest using Sentinel-2 and GLCM texture features: A case study for the Lousã region, Portugal," *Remote Sensing*, vol. 14, no. 18, 2022. doi:10.3390/rs14184585.

[9] L. Costanza *et al.*, "Predicting olive tree chlorophyll fluorescence using explainable AI with Sentinel-2 imagery in Mediterranean environments," *Applied Sciences*, vol. 15, no. 5, 2025. doi:10.3390/app15052746.

[10] A. E. Maxwell, T. A. Warner, and F. Fang, "Implementation of machine-learning classification in remote sensing: An applied review," *International Journal of Remote Sensing*, vol. 39, no. 9, pp. 2784–2817, 2018. doi:10.1080/01431161.2018.1433343.

[11] S. K. Abebaw Alem, "Machine learning approaches for land classification," in *Proceedings of the IEEE 8th International Conference on Reliability, Infocom Technologies and Optimization (ICRITO)*, 2020. doi:10.1109/ICRITO48877.2020.9197824.

[12] W. Utama, R. F. Indriani, M. Hermana, I. M. Anjasmara, S. A. Garini, and D. P. N. Putra, "Towards improving sustainable water management in geothermal fields: SVM and RF land use monitoring," *Journal of Human, Earth, and Future*, vol. 5, no. 2, pp. 216–242, 2024. doi:10.28991/HEF-2024-05-02-06.

[13] R. K. Singh *et al.*, "A machine learning-based classification of Landsat images to map land use and land cover of India," *Remote Sensing Applications: Society and Environment*, vol. 24, 2021. doi:10.1016/j.rsase.2021.100624.

[14] M. Wakulińska and A. Marcinkowska-Ochtyra, "Multi-temporal Sentinel-2 data in classification of mountain vegetation," *Remote Sensing*, vol. 12, no. 17, 2020. doi:10.3390/rs12172696.

[15] S. Rina *et al.*, "Application of machine learning to tree species classification using active and passive remote sensing: A case study of the Duraer forestry zone," *Remote Sensing*, vol. 15, no. 10, 2023. doi:10.3390/rs15102596.

[16] T. Lees, G. Tseng, C. Atzberger, S. Reece, and S. Dadson, "Deep learning for vegetation health forecasting: A case study in Kenya," *Remote Sensing*, vol. 14, no. 3, 2022. doi:10.3390/rs14030698.

[17] M. Zhang, D. Li, G. Li, and D. Lu, "Vegetation classification in a subtropical region with Sentinel-2 time series data and deep learning," *Geo-Spatial Information Science*, vol. 28, no. 1, pp. 145–163, 2025. doi:10.1080/10095020.2024.2336604.

[18] G. Aziz *et al.*, "Remote sensing-based forest cover classification using machine learning," *Scientific Reports*, vol. 14, no. 1, 2024. doi:10.1038/s41598-023-50863-1.

[19] K. L. Du, B. Jiang, J. Lu, J. Hua, and M. N. S. Swamy, "Eploring kernel machines and support vector machines: Princples, techniques, and future directions," *Mathematics*, vol. 12, no. 24, 2024. doi:10.3390/math12243935.